PNAS RESEARCH ARTICLE | CELL BIOLOGY OPEN ACCESS

Redox metabolism maintains the leukemogenic capacity and drug resistance of AML cells

Dan Huang[a,1], Changcheng Zhang[b,1], Ming Xiao[c,1], Xie Li[b,1], Weicai Chen[b,1], Yu Jiang[a], Yamin Yuan[a], Yaping Zhang[a], Yejun Zou[b], Lei Deng[b], Yang Wang[d], Yuying Sun[b], Wenping Dong[b], Zhuo Zhang[b], Li Xie[a], Zhuo Yu[a], Chiqi Chen[a], Ligen Liu[a], Jing Wang[d], Yi Yang[b,2], Jie Yang[c,2], Yuzheng Zhao[b,e,2], and Junke Zheng[a,f,g,2]

Edited by David T. Scadden, Harvard Stem Cell Institute, Boston, MA; received June 28, 2022; accepted February 21, 2023 by Editorial Board Member Rakesh K. Jain

Rewiring of redox metabolism has a profound impact on tumor development, but how the cellular heterogeneity of redox balance affects leukemogenesis remains unknown. To precisely characterize the dynamic change in redox metabolism in vivo, we developed a bright genetically encoded biosensor for H_2O_2 (named HyPerion) and tracked the redox state of leukemic cells in situ in a transgenic sensor mouse. A H_2O_2-low (HyPerion-low) subset of acute myeloid leukemia (AML) cells was enriched with leukemia-initiating cells, which were endowed with high colony-forming ability, potent drug resistance, endosteal rather than vascular localization, and short survival. Significantly high expression of malic enzymes, including ME1/3, accounted for nicotinamide adenine dinucleotide phosphate (NADPH) production and the subsequent low abundance of H_2O_2. Deletion of malic enzymes decreased the population size of leukemia-initiating cells and impaired their leukemogenic capacity and drug resistance. In summary, by establishing an in vivo redox monitoring tool at single-cell resolution, this work reveals a critical role of redox metabolism in leukemogenesis and a potential therapeutic target.

H_2O_2 biosensor | redox metabolism | AML | leukemia-initiating cells | drug resistance

Significance

By using the H_2O_2 sensor (termed as HyPerion), we unravel a unique redox metabolic preference in maintaining the reactive oxygen species (ROS) level of acute myeloid leukemia (AML) cells. HyPerion-low AML cells have enhanced leukemogenic capacities, are enriched for functional leukemia-initiating cells, tend to localize in the endosteal niche, and are more resistant to chemotherapy, which may be fine-tuned by malic enzyme ME1/3. Targeting ME1/3 can efficiently delay the AML development and overcome the drug resistance.

Acute myeloid leukemia is a malignant hematopoietic disorder that originates from hematopoietic stem progenitor cells and commonly occurs in adults, especially in elderly patients. The overall 5-y survival rate ranges from 5 to 40% (1, 2). Currently, chemotherapy is the most effective way to treat different types of acute myeloid leukemia (AML), but relapse or drug resistance occurs in more than 30% of patients (3). It has been reported that there may exist one small fraction of the cell population, termed leukemia-initiating cells (LICs), which are responsible for the initiation, progression, relapse, and drug resistance of AML (4, 5).

Recently, increasing evidence has shown that different metabolic fuels, including glucose, amino acids, fatty acids, nuclear acids, and vitamins, fine-tune the fates of AML cells or LICs, such as self-renewal, differentiation, localization in the bone marrow (BM) niche, and drug resistance (6–7). Moreover, redox metabolism, especially the reactive oxygen species (ROS) level, has been reported to be connected with the leukemogenic capacities of AML cells (8–9). A moderate ROS level promotes tumor initiation as a proliferative signaling messenger, while a high ROS level may trigger oxidative stress and cell death.

Certain levels of ROS are balanced between ROS generation and the antioxidative system, which is known to be required for the proliferation, differentiation, genomic stability, drug resistance, and immune escape of leukemic cells. For example, by using a fluorescent chemical probe, it has been reported that functional LICs have relatively low ROS levels and oxygen consumption rates (10). Quiescent LICs have relatively low energy requirements and low levels of ROS and are more resistant to cytarabine treatment (11). *IDH1/2* mutations lead to the upregulation of ROS levels resulting from increased NADPH consumption, followed by the initiation of AML (12). *FLT3-ITD* mutations can cause an increase in ROS levels, which further result in the genetic instability of AML cells (13). However, how ROS level is maintained and contribute to the control of LIC fate during leukemogenesis is still not fully understood.

The components of ROS include hydrogen peroxide (H_2O_2), superoxide anion ($O_2^{\bullet-}$), and hydroxyl radical ($OH^{\bullet}$), which are mainly produced by several key biological pathways, including oxidative phosphorylation, NADPH oxidase activities, and cellular oxidant-generating systems. Among all ROS components, H_2O_2 has been considered the most important and plays key roles in various physiological and pathological activities of many cell types (14, 15). ROS components in cells are extremely unstable and are still

Author contributions: D.H., C.Z., M.X., X.L., W.C., J.Y., and J.Z. designed research; D.H., C.Z., M.X., X.L., W.C., Y.J., Y. Yuan, Y. Zhang, Y. Zou, L.D., Y.W., Y.S., W.D., Z.Z., L.X., Z.Y., C.C., L.L., J.W., Y. Yang, J.Y., Y. Zhao, and J.Z. performed research; Y.J., Y. Yuan, Y. Zhang, Y. Zou, L.D., Y.W., Y.S., W.D., Z.Z., L.X., Z.Y., C.C., L.L., J.W., Y. Yang, and Y. Zhao contributed new reagents/analytic tools; D.H., C.Z., M.X., X.L., W.C., J.Y., and J.Z. analyzed data; and D.H., C.Z., M.X., X.L., W.C., J.Y., and J.Z. wrote the paper.

The authors declare no competing interest.

This article is a PNAS Direct Submission. D.T.S. is a guest editor invited by the Editorial Board.

[1]D.H., C.Z., M.X., X.L., and W.C. contributed equally to this work.

[2]To whom correspondence may be addressed. Email: yiyang@ecust.edu.cn, yangjieyj@shsmu.edu.cn, yuzhengzhao@ecust.edu.cn, or zhengjunke@shsmu.edu.cn.

This article contains supporting information online at https://www.pnas.org/lookup/suppl/doi:10.1073/pnas.2210796120/-/DCSupplemental.

Published March 22, 2023.

difficult to measure dynamically. For example, H_2O_2 exists for only a few seconds in cells (16) and is then catabolized into H_2O through peroxiredoxins, glutathione peroxidases, or catalase (17). Currently, a few methods have been established for ROS measurement. Among them, dichlorofluorescein (DCF) derivatives are widely used to detect intracellular ROS. DCF derivatives, however, are nonspecific, usually irreversible, operationally tedious, and susceptible to artifacts (18), thus rendering them difficult to monitor in vivo.

Genetically encoded fluorescent sensors capable of live-cell or in vivo monitoring have been developed for various metabolites (19, 20). Recently, we, together with our collaborators, have developed several metabolic sensors, including SoNar (NADH/NAD^+ sensor) (21, 22), iNap1 (NADPH sensor) (23, 24), and a branched-chain amino acid sensor (25), and unraveled the tight connection between metabolic status and fate commitments of AML cells or LICs by these ultrasensitive metabolic sensors. The HyPer sensor family is often used to monitor H_2O_2 in living cells, but in vivo monitoring remains challenging due to the limitation of brightness. Due to the highly dynamic nature and important functions of H_2O_2, a better H_2O_2 sensor with high brightness would be highly favorable, and a transgenic animal model with sensor expression should be a valuable tool for the mechanistic study of redox biology. In this study, we developed a bright, genetically encoded H_2O_2 sensor, named HyPerion, and engineered HyPerion-expressing transgenic mice. Utilizing these powerful tools, we found that the H_2O_2 level was a critical determining factor of functional LICs and AML development.

Results

Bright HyPerion Sensor Enables Real-Time and In Vivo Monitoring of H_2O_2. To engineer a bright sensor, we used HyPer3, a cpYFP-based H_2O_2 sensor with improved performance (26), as a template and performed mutational screening (27, 28). According to the brightness and fluorescence responsiveness, a HyPer3 variant with the Y131F/S262R/N337T mutation showed a favorable performance, which was denoted HyPerion (Fig. 1*A* and *SI Appendix*, Fig. S1*A*). HyPerion had two excitation maxima at approximately 415 nm and 500 nm and one emission peak near 514 nm (Fig. 1*B* and *SI Appendix*, Fig. S1 *B* and *C*). Upon H_2O_2 binding, HyPerion showed a ~2.1-fold increase and ~1.7-fold decrease in fluorescence when excited at 485 nm and 420 nm, respectively (Fig. 1*C*). More importantly, HyPerion displayed ~4.0-fold, 3.2-fold, and 4.3-fold higher brightness than HyPer1, HyPer2, and HyPer3, respectively, when excited at 485 nm and 2.0-fold, 2.1-fold, and 2.3-fold higher brightness than HyPer1, HyPer2, and HyPer3, respectively, when excited at 420 nm in *Escherichia coli* BL21 cells (Fig. 1*D*). In mammalian cells, the brightness of HyPerion was up to 13.8- and 4.2-fold higher at 485 and 420-nm excitation, respectively, than HyPer3 (Fig. 1*E*).

We then used HyPerion to monitor the H_2O_2 level in living cells. In HeLa cells, HyPerion manifested a dynamic change of ~fourfold in the ratio of fluorescence when excited at 488 nm and 405 nm individually ($F_{488/405}$ for short) in response to H_2O_2. The $F_{488/405}$ ratio was sharply reduced upon subsequent treatment with DTT (Fig. 1*F*). To further establish an in vivo monitoring technology, we used the CRISPR–Cas9 technique to construct HyPerion transgenic mice (knock-in mice for short) (*SI Appendix*, Fig. S1*D*). We then confirmed the transcription of HyPerion in various organs, showing the highest levels in the lung, kidney, muscle, and brain and the lowest levels in the liver, spleen, and intestine (*SI Appendix*, Fig. S1*E*). We also carried out fluorescence imaging of whole-body HyPerion mice with shaved backs and found high intensities at 430 nm and 500 nm excitation (Fig. 1*G*). Finally, the intensity of F_{405} and F_{488} of HyPerion in frozen sections of multiple organs from HyPerion mice was observed under a confocal microscope (Fig. 1*H*). To examine HyPerion's performance in living organisms, we carried out in vivo imaging to observe the redox response to acute liver injury. Upon the administration of the drug acetaminophen or the biotoxin CCl_4, $F_{488/405}$ of the mouse liver increased from 0.48 to 1.02 or 1.07, while N-acetyl cysteine (NAC) pretreatment obviously prevented the increase in the ratio (Fig. 1*I*). The performance of HyPerion in peripheral blood cells was also tested. The fluorescence of the blood cells separated from 8-wk-old HyPerion mice was obviously higher than that of wild-type (WT) mice (*SI Appendix*, Fig. S1 *F* and *G*). In response to H_2O_2 and its scavenger DTT, the $F_{488/405}$ ratio in lymphocytes and monocytes was increased and decreased, respectively (Fig. 1*J*). Taken together, these data indicate that the HyPerion sensor displays a superior response, high fluorescence intensity, and large dynamic range and is very useful for the real-time tracking of redox metabolism in living cells and in vivo.

HyPerion Can Be Used to Precisely Monitor the ROS Levels of Hematopoietic Cells. We then performed single-cell analysis of hematopoietic cells using HyPerion transgenic mice and found that the total BM cells were very heterogeneous and could be divided into three distinct populations with low, middle, and high HyPerion ratios by confocal microscopy (Fig. 2 *A* and *B*). $HyPerion^+$ BM cells and multiple lineages could sensitively respond to the stimulation by either H_2O_2 or its scavenger DTT and NAC (Fig. 2 *C* and *D* and *SI Appendix*, Fig. S2 *A* and *B*). The sequential treatment with H_2O_2 and DTT further revealed that these HyPerion ratios first markedly increased and then gradually decreased over time (Fig. 2 *E* and *F* and Movie S1). Moreover, heterogeneous populations with low-high HyPerion ratios were observed both in adult (Fig. 2 *G–I*) and fetal liver hematopoietic stem cells (HSCs) (*SI Appendix*, Fig. S2 *C–E*) purified from HyPerion transgenic mice, which could sensitively respond to the stimulation of H_2O_2, DTT, and NAC. Interestingly, the ratios of HyPerion were much lower in long term HSCs (LT-HSCs) and short term HSCs (ST-HSCs) than those in multipotent progenitor (MPP) (*SI Appendix*, Fig. S2 *F* and *G*). Among all the hematopoietic progenitor cells, we demonstrated that common myeloid progenitor (CMP) and common lymphocyte progenitor (CLP) displayed relatively low HyPerion ratios, while granulocyte-monocyte progenitor (GMP) and megakaryocyte-erythroid progenitor (MEP) exhibited relatively high HyPerion ratios (*SI Appendix*, Fig. S2*H*). These data indicate that H_2O_2 levels may be dynamically changed in different subtypes of hematopoietic stem/progenitor cells (HSPCs) and tightly connected with their cell fates. Importantly, the HyPerion ratios of BM cells in cranium were promptly increased or decreased upon stimulation with H_2O_2 and DTT as determined by a surrogate in vivo assay (*SI Appendix*, Fig. S2 *I* and *J* and Movies S2 and S3).

HyPerion Can Dynamically Indicate the ROS Levels of AML Cells. We then further established a murine AML model by ectopic expression of MLL-AF9 in purified HSPCs from HyPerion transgenic mice and transplanted them into recipient mice. We found heterogeneity in HyPerion ratios within AML cells from the Hyperion transgenic model, which could further be divided into HyPerion-low, middle (mid), and high populations (Fig. 3 *A* and *B*). Up to a fourfold range of changes in HyPerion ratios was observed in these AML cells upon treatment with H_2O_2 and DTT as evaluated either by confocal microscopy (Fig. 3 *C* and *D*) or flow cytometric analysis (*SI Appendix*, Fig. S3 *A* and *B*). Interestingly,

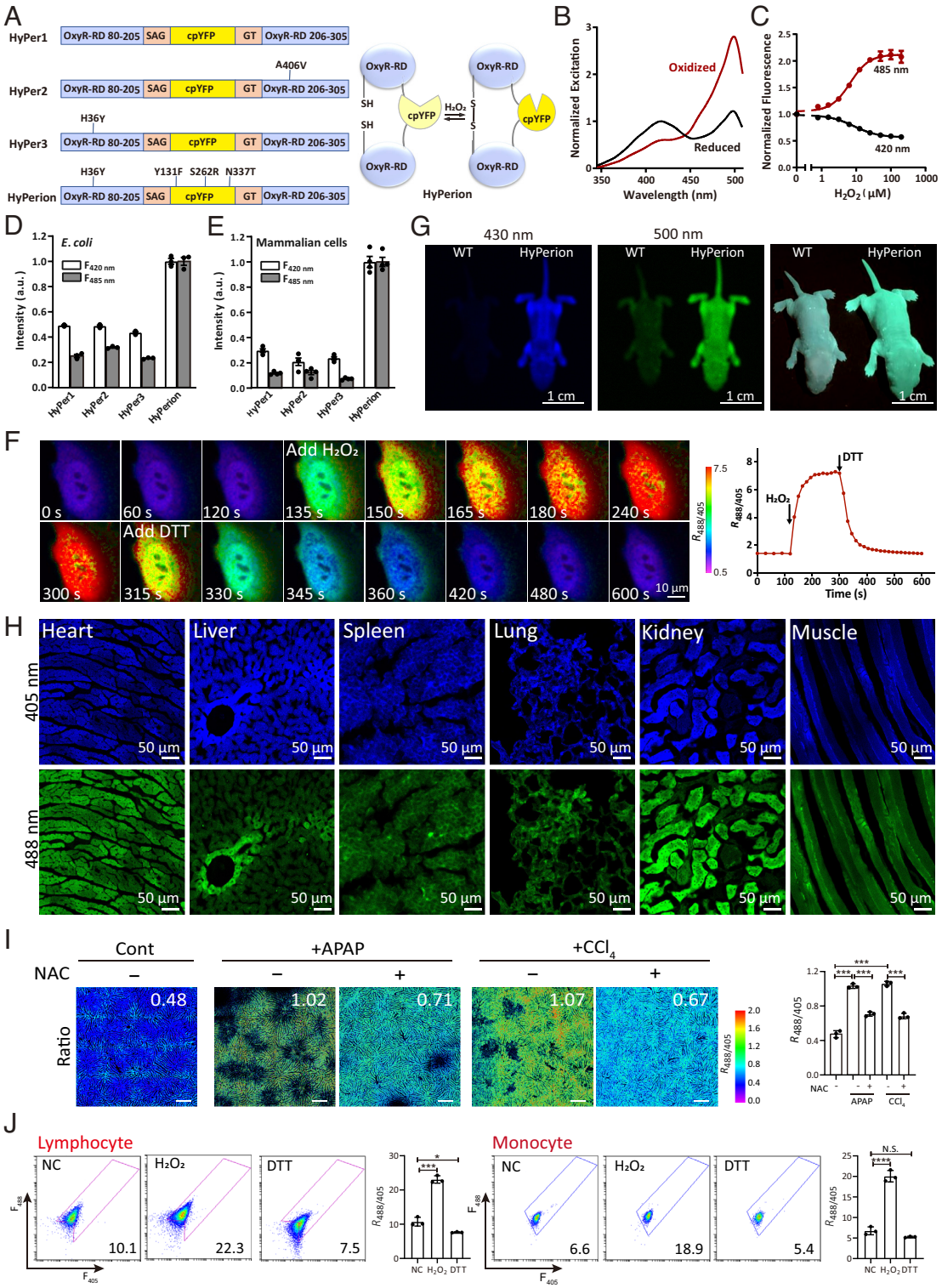

Fig. 1. The bright HyPerion sensor enables real-time and in vivo monitoring of H_2O_2. (*A*, *Left*), schematic representation of the hydrogen peroxide (H_2O_2) sensors HyPer1, HyPer2, HyPer3, and HyPerion. HyPerion was generated by three point mutations Y1F, S132R, and N207T in cpYFP corresponding to Y131F, S262R, and N337T in HyPer3 (HyPer with H36Y). *Right*, HyPerion contains two critical Cys residues, C199 and C208, in WT OxyR. Exposure of the sensor to H_2O_2 induces a C199 bond with C208 and forms a disulfide bond. As a result, dramatic changes occur in protein conformation and fluorescence. These changes are reversible. (*B*) Excitation spectra of HyPerion under reduced conditions (black, 10 mM dithiothreitol (DTT)) and oxidized conditions (dark red, 500 μM H_2O_2). The excitation spectrum recorded at an emission wavelength of 530 nm has maxima at 417 and 500 nm. Data are normalized to peak intensity at 417 nm in the reduced condition. (*C*) Fluorescence intensities of HyPerion with excitation at 485 nm or 420 nm in the presence of H_2O_2 and emission at 528 nm. Data are normalized to the fluorescence in the reduced condition (10 mM DTT) (n = 3). (*D* and *E*) Fluorescence comparison of HyPerion with HyPer1, HyPer2, and HyPer3 excitation at 485 nm and 420 nm, respectively, in *E. coli* BL21 cells (*D*) and in HeLa cells (*E*). (*F*) Fluorescence images and quantification of HyPerion in HeLa cells upon the addition of 100 μM H_2O_2 and 5 mM DTT in succession at the indicated times. (Scale bars, 10 μm.) (*G*) In vivo fluorescence imaging of neonatal HyPerion transgenic mice and WT mice excited at 430 and 500 nm (*Left* and *Middle*) and comparison of neonatal HyPerion transgenic mice with WT mice under UV illumination (395 nm) (*Right*). (Scale bar, 1 cm.) (*H*) HyPerion fluorescence was examined in different tissues/organs of either WT or HyPerion transgenic mice by confocal microscopy. (Scale bar, 50 μm.) (*I*) In vivo fluorescence images (*Left*) and quantification (*Right*) of HyPerion in acute liver injury mice. Images are pseudocolored according to $R_{488/405}$. (Scale bar, 100 μm.) (*J*) Representative flow cytometric analysis and quantification of HyPerion in peripheral blood lymphocytes and monocytes from HyPerion mice. The cells were treated with 100 μM H_2O_2 or 5 mM DTT. Data are represented as means ± SD. *P < 0.05, ***P < 0.001***.

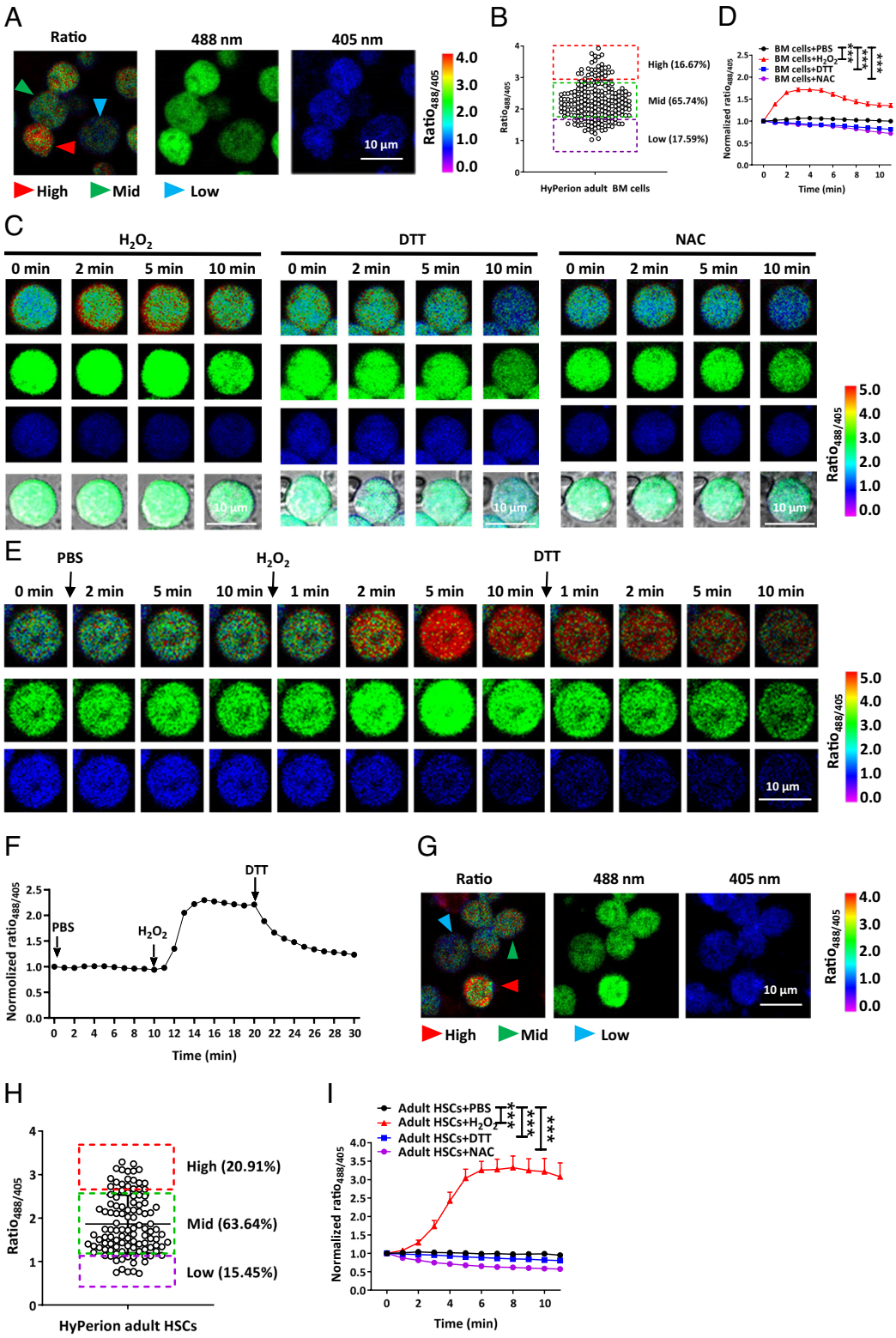

Fig. 2. HyPerion can be used to precisely monitor H_2O_2 levels in hematopoietic cells. (*A*) HyPerion$^+$ BM cells were subjected to the evaluation of the ratios of HyPerion fluorescence ($F_{488/405}$), and representative images are shown. (*B*) Quantification of HyPerion$^+$ BM cells with different ratios of HyPerion fluorescence in Panel *A*. A total of 216 BM cells were examined. (n = 3). HyPerion-low (ratio < 1.5), HyPerion-mid (ratio 1.5 to 2.5), and HyPerion-high cells (ratio > 2.5) were defined accordingly. (*C*) Representative images of the ratios of HyPerion fluorescence with excitation at 405 nm and 488 nm ($F_{488/405}$) in BM cells at the indicated time points upon H_2O_2, DTT, or NAC stimulation. (*D*) Quantification of the ratios of HyPerion fluorescence in Panel *C*. A total of 80 to 100 BM cells were analyzed (n = 3). (*E*) Representative images of the ratios of HyPerion fluorescence in HyPerion$^+$ BM cells upon sequential treatments with PBS, H_2O_2, and DTT. (*F*) Quantification of the ratios of HyPerion fluorescence in Panel *E*. A total of 30 to 40 HyPerion$^+$ BM cells were analyzed (n = 3). (*G*) The ratios of HyPerion fluorescence ($F_{488/405}$) were determined in CD45$^+$HyPerion$^+$ adult HSCs by confocal microscopy, and representative images are shown. (*H*) Quantification of the ratios of HyPerion fluorescence in Panel *G*. A total of 110 adult HSCs were examined (n = 3). (*I*) CD45$^+$ HyPerion$^+$ adult HSCs were treated with PBS, H_2O_2, DTT, or NAC, followed by the measurement of the ratios of HyPerion fluorescence at the indicated time points. A total of 16 to 28 CD45$^+$HyPerion$^+$ adult HSCs were analyzed (n = 3). Data are represented as means ± SD. ***P < 0.001***.

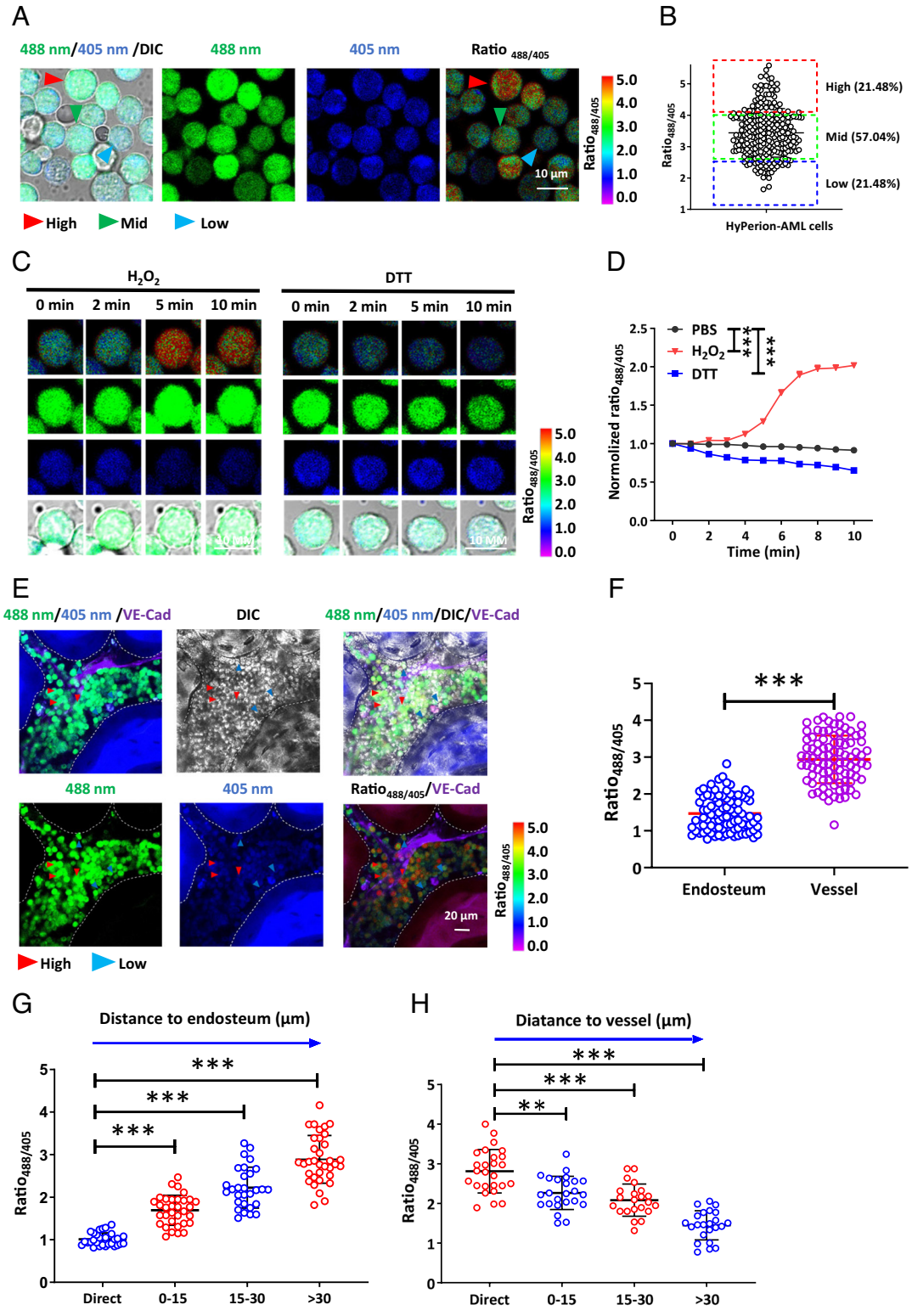

Fig. 3. HyPerion can dynamically indicate H_2O_2 levels in AML cells. (*A*) HyPerion$^+$ AML cells were subjected to the evaluation of the ratios of HyPerion fluorescence ($F_{488/405}$), and representative images are shown. (*B*) Quantification of HyPerion$^+$ AML cells with different ratios of HyPerion fluorescence in Panel *A*. A total of 257 BM cells were examined (n = 3). HyPerion-low (ratio < 2.5), HyPerion-mid (ratio 2.5 to 4), and HyPerion-high cells (ratio > 4) were defined accordingly. (*C*) Representative images of the ratios of HyPerion fluorescence with excitation at 405 nm and 488 nm ($F_{488/405}$) in AML cells at the indicated time points upon H_2O_2 or DTT stimulation. (*D*) Quantification of the ratios of HyPerion fluorescence in Panel *C*. A total of 60 to 100 AML cells were analyzed (n = 3). (*E–H*) Representative images of the localizations of HyPerion-low and HyPerion-high AML cells in the vascular niche labeled by anti-VE-cadherin antibodies (VE-Cad, purple) or in the endosteal niche (dashed lines) and their ratios of HyPerion fluorescence ($F_{488/405}$) are shown. A total of 180 to 200 HyPerion$^+$ BM cells were analyzed (n = 3). Data are represented as means ± SD. ***$P < 0.001$***.

much higher HyPerion ratios were observed in the vascular niche than in the endosteal niche (Fig. 3 *E* and *F*). We also noticed that the higher the HyPerion fluorescence ratios AML cells had, the closer these cells localized to the vascular niche in BM (Fig. 3 *G* and *H*), indicating that the ROS levels may be tightly connected with the cell fates of AML cells. Moreover, the HyPerion ratios increased

much more slowly in AML cells in the vascular niche than those in the endosteal niche upon H_2O_2 treatment (*SI Appendix*, Fig. S3 *C* and *D*). In contrast, the HyPerion ratios were reduced much faster in AML cells in the vascular niche than those in the endosteal niche upon DTT treatment (*SI Appendix*, Fig. S3 *E* and *F*).

HyPerion-low AML Cells Have Enhanced Leukemogenic Capacities and Are Enriched for LICs. To test the functional difference between HyPerion-low and HyPerion-high cell populations, we isolated HyPerion-low and HyPerion-high cells and further evaluated their HyPerion ratios by confocal microscopy and flow cytometry (Fig. 4 *A*–*C*). Interestingly, HyPerion-low cells had much higher frequencies of immunophenotypic Mac-1$^+$c-Kit$^+$ LICs than HyPerion-high LICs, as determined by flow cytometric analysis (Fig. 4*D*). An in vitro functional colony-forming assay also showed that HyPerion-low cells gave rise to more colonies, as well as total derived leukemia cell numbers (Fig. 4 *E*–*G*). In vivo

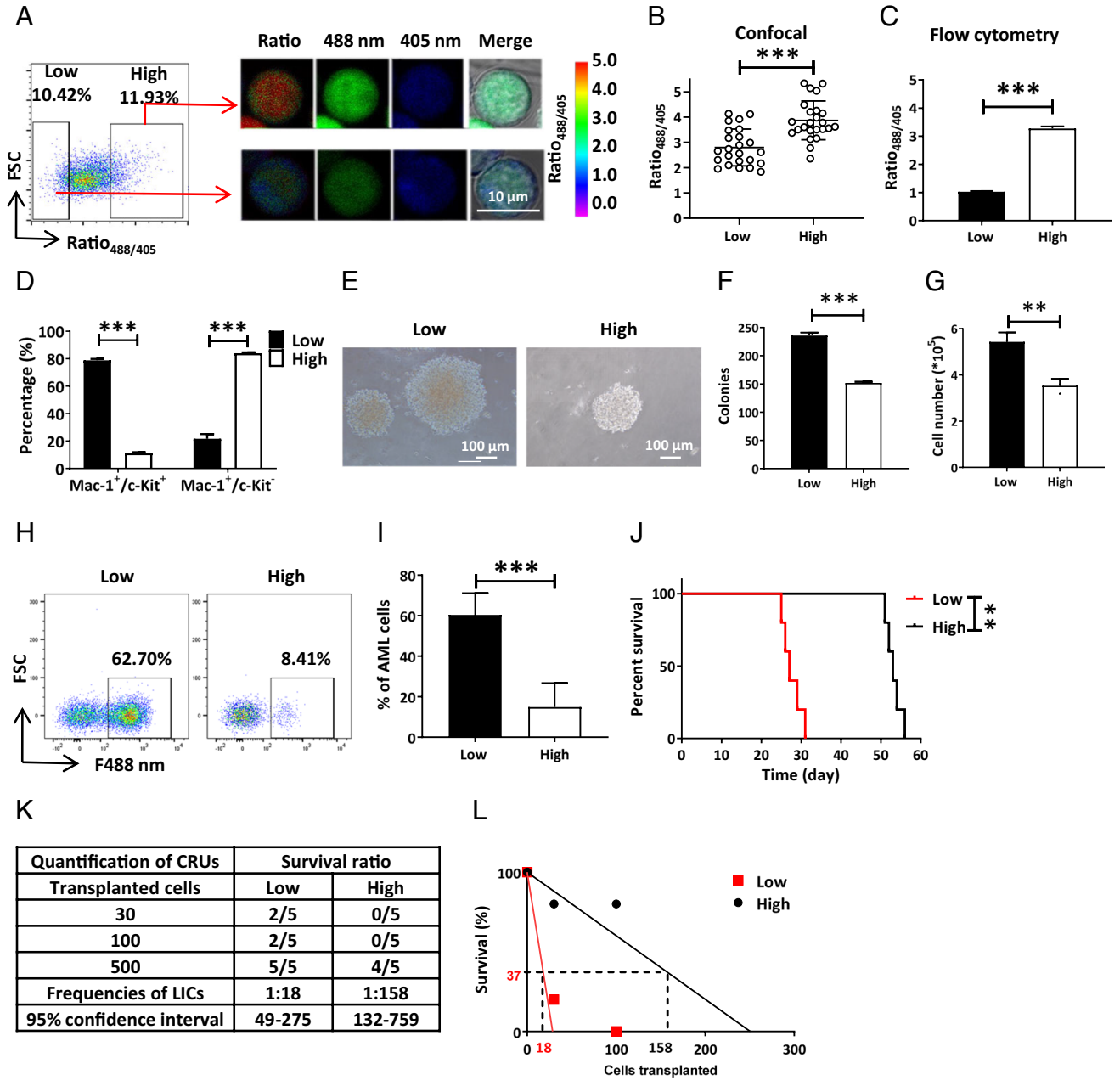

Quantification of CRUs	Survival ratio	
Transplanted cells	Low	High
30	2/5	0/5
100	2/5	0/5
500	5/5	4/5
Frequencies of LICs	1:18	1:158
95% confidence interval	49-275	132-759

Fig. 4. HyPerion-low AML cells have enhanced leukemogenic capacities and are enriched for functional LICs. (*A*) FACS-purified HyPerion-low and HyPerion-high AML cells were evaluated for the ratios of HyPerion fluorescence with excitation at 405 nm and 488 nm by confocal microscopy, and representative images are shown. (*B* and *C*) Quantification of HyPerion's fluorescence ($F_{488/405}$) in Panel *A* as measured by either confocal microscopy (*B*, n = 3) or flow cytometric analysis (*C*, n = 3). (*D*) Quantification of Mac-1$^+$c-Kit$^+$ immunophenotypical LICs in HyPerion-low and HyPerion-high AML cells (n = 3). (*E*) Representative images for the colonies derived from HyPerion-low and HyPerion-high cells cultured in methylcellulose medium (colony forming unit (CFU) assay). (Scale bar, 100 μm.) (*F* and *G*) Quantification of colony numbers and total cell numbers derived from HyPerion-low and HyPerion-high AML cells in Panel *E* (n = 3). (*H*) Representative flow cytometric analysis of the leukemia cell frequencies in the peripheral blood of recipients receiving HyPerion-low and HyPerion-high AML cells. (*I*) Quantification of the data in Panel *H* (n = 5). (*J*) Overall survival was determined in recipients receiving HyPerion-low and HyPerion-high AML cells in one representative experiment (n = 5). (*K* and *L*) The indicated cell numbers of HyPerion-low and HyPerion-high AML cells were injected into recipients in one representative experiment (n = 5), and functional LIC frequencies were calculated according to the survival rates using L-Calc software. Experiments were repeated independently three times. Data are represented as means ± SD. $^{**}P < 0.001$, $^{***}P < 0.001$.

transplantation experiments consistently showed that the recipient mice receiving HyPerion-low cells had a more severe leukemia burden than HyPerion-high control mice, as displayed by higher leukemia cell frequencies in peripheral blood (62.70% vs. 8.41%, Fig. 4 *H* and *I*), enhanced infiltration in spleens and livers (*SI Appendix*, Fig. S4 *A–C*), and reduced overall survival (53 d vs. 27 d, Fig. 4*J*). No significant difference in differentiation capacity was found between these HyPerion-low and HyPerion-high cells (*SI Appendix*, Fig. S4 *D* and *E*). Limiting dilution assays further showed that HyPerion-low cells contained ~ninefold higher functional LIC numbers than HyPerion-high cells (Fig. 4 *K* and *L*), suggesting that HyPerion-low cells were enriched for more LICs. Similar to our previous findings in MLL-AF9 mouse model, we showed that AML1-ETO9a$^+$ HyPerion-low AML cells (another murine AML model) contained ~2.5-fold greater functional LIC numbers than HyPerion-high cells (*SI Appendix*, Fig. S4*F*), indicating that HyPerion-low cells are enriched for more functional LICs and is not limited to the MLL-AF9 model.

Meanwhile, the HyPerion-low cells had much lower ATP levels (*SI Appendix*, Fig. S4*G*), mitochondrial membrane potential (*SI Appendix*, Fig. S4 *H* and *I*), and intermediate metabolites of oxidative phosphorylation (succinate and alpha-ketoglutarate, *SI Appendix*, Fig. S4 *J* and *K*) but higher levels of NADPH (*SI Appendix*, Fig. S4 *L* and *M*) and intermediate metabolites for glycolysis (pyruvate and lactate, *SI Appendix*, Fig. S4 *N* and *O*). We had also determined the intracellular ROS level with a general ROS dye, CellROX, and showed that HyPerion-high AML cells had ~1.7-fold greater ROS levels than that of HyPerion-low counterparts in a MLL-AF9 AML model (*SI Appendix*, Fig. S4 *P* and *Q*). HyPerion-low AML cells had higher levels of extracellular acidification rate (ECAR) and lower levels of O_2 consumption rate (OCR) compared to that of HyPerion-high cells as determined by a Seahorse assay (*SI Appendix*, Fig. S4 *R* and *S*). In addition, a metabolic flux analysis with 13C-labeled glucose showed that HyPerion-low AML cells had an enhanced glycolysis level, but decreased OXPHOS level compared to that of HyPerion-high AML cells, as indicated by the related intermediate metabolites and the ratio of lactate/alphaKG or lactate/succinate (*SI Appendix*, Fig. S4 *T–V*). These data suggested that the HyPerion-low cells are prone to relying on glycolysis rather than OXPHOS.

To test whether stemness state impacts the output from their biosensor, we ectopically expressed the MLL-AF9 oncogene in purified GMP (Lin$^-$Sca$^-$1$^-$c-Kit$^+$CD16/32$^+$CD34$^+$) and HSCs (Lin$^-$Sca-1$^+$c-Kit$^+$) cells from HyPerion transgenic mice and transplanted them into recipient mice to establish the murine AML model. The leukemia development was much faster in the recipient mice receiving HyPerion-low AML cells from either GMP (*SI Appendix*, Fig. S4 *W* and *X*) or HSCs (*SI Appendix*, Fig. S4 *Y* and *Z*) transduced leukemia model, indicating that the redox metabolism (but not stemness state) may be important for promoting leukemogenesis derived from GMP, HSCs, and Lin$^-$ BM cells.

ME1/3 Fine-Tunes ROS Levels to Maintain the Leukemogenic Capacities of HyPerion-Low AML Cells. To delineate the underlying mechanisms that control ROS levels in AML cells, HyPerion-low and HyPerion-high cells were purified and subjected to quantitative RT-PCR. We measured all the critical genes related to ROS clearance and generation, including *Glrx1*, *Glrx2*, *Glrx3*, *Grx1*, *Sod1*, *Sod2*, *Txn1*, *Txn2*, *Txnrd1*, *Txnrd2*, *Txnrd3*, *Prdx1*, *Me1*, *Me2*, *Me3*, *Mthfd1*, *Mthfd2*, *Idh1*, *Idh2*, *Pgd*, *G6pd*, *Nnt*, *Mdh1*, *Cox17*, and *Uqcrq*, and noticed that *Me1* and *Me3* expression levels in HyPerion-low cells were 16.58- and 7.65-fold higher than those in HyPerion-high cells (Fig. 5*A*), indicating that they may serve as potential downstream targets. ME1 and ME3 mediate the conversion of malate to pyruvate, accompanied by the generation of NADPH, which are the critical cofactors involved in the detoxification of H_2O_2. Consistently, knockdown of *Me1* in AML cells by shRNAs (sh*Me1*#1 and sh*Me1*#3, *SI Appendix*, Fig. S5*A*) led to a notable delay in leukemogenesis in recipient mice, as evidenced by the reduced leukemia cell frequencies in peripheral blood (Fig. 5 *B* and *C*), decreased infiltration in spleens and livers (Fig. 5*D*), and markedly extended overall survival (22 d for the scrambled group and 32 or 38 for the *Me1*-knockdown group, Fig. 5*E*). *Me1*-knockdown AML cells exhibited much higher HyPerion ratios than scrambled cells, as determined by either confocal microscopy (*SI Appendix*, Fig. S5 *B* and *C*) or flow cytometric analysis (*SI Appendix*, Fig. S5 *D* and *E*). Moreover, in the BM niche, the overall HyPerion ratios of *Me1*-knockdown AML cells were much higher than those of scrambled cells (Fig. 5 *F* and *G*).

We then further knocked down *Me3* in AML cells by shRNAs (sh*Me3*#1 and sh*Me3*#4, *SI Appendix*, Fig. S5*F*) and demonstrated that knockdown of *Me3* also led to a marked decrease in leukemia cell frequencies in peripheral blood (*SI Appendix*, Fig. S5*G*) and extended survival in recipient mice (*SI Appendix*, Fig. S5*H*). Similar to the findings in *Me1*-knockdown AML cells, the HyPerion ratios were also notably up-regulated in *Me3*-knockdown cells compared to scrambled cells (*SI Appendix*, Fig. S5 *I* and *J*). Meanwhile, the overall HyPerion ratios of *Me3*-knockdown AML cells in the BM niche were much higher than those of scrambled cells (*SI Appendix*, Fig. S5 *K* and *L*). These results indicate that both ME1 and ME3 are involved in the generation of NADPH to down-regulate the H_2O_2 levels and maintain the leukemogenic abilities of AML cells. Consistently, knockdown of *Me1/3* led to the notable decrease in both NADPH level and NADPH/NADP ratio in AML cells (*SI Appendix*, Fig. S5 *M–P*).

HyPerion-low AML Cells Are More Resistant to Chemotherapy. To reveal the potential connection between drug resistance and ROS levels, HyPerion-low cells were first subjected to in vitro treatment with the indicated doses of Ara-C, a first-line chemotherapeutic agent, which clearly showed that HyPerion-low cells were more resistant to Ara-C treatment than HyPerion-high cells (Fig. 6*A*). We then treated leukemic mice with Ara-C and ADM (induction chemotherapy, iCT) for 3 d and found that the HyPerion ratios of AML cells in the BM niche were much lower than those in the control group (Fig. 6 *B* and *C*). An in vitro functional colony assay further showed that AML cells isolated from the recipient mice pretreated with Ara-C could give rise to more colonies, as well as higher derived cell numbers (Fig. 6 *D–F*). Consistently, HyPerion-low cells had ~fourfold or fivefold higher mRNA levels of *Me1* or *Me3* than HyPerion-high cells, respectively. Interestingly, the difference in *Me1* and *Me3* mRNA levels between HyPerion-low and HyPerion-high cells was further increased ~eightfold or tenfold upon treatment with Ara-C (Fig. 6*G*), indicating that *Me1* and *Me3* may serve as potential targets for the drug resistance of AML cells.

The leukemia development was also significantly delayed in the recipients receiving *Me1*-knockdown and *Me3*-knockdowm AML cells after treatment with iCT, as displayed by the reduced leukemia cell frequencies in peripheral blood (*SI Appendix*, Fig. S6 *A–F*) and extended overall survival compared to their counterparts. We also treated the leukemic mice with iCT and $LaCl_3$ (a competitive inhibitor of MEs) and demonstrated that combined treatment could further inhibit AML development compared to

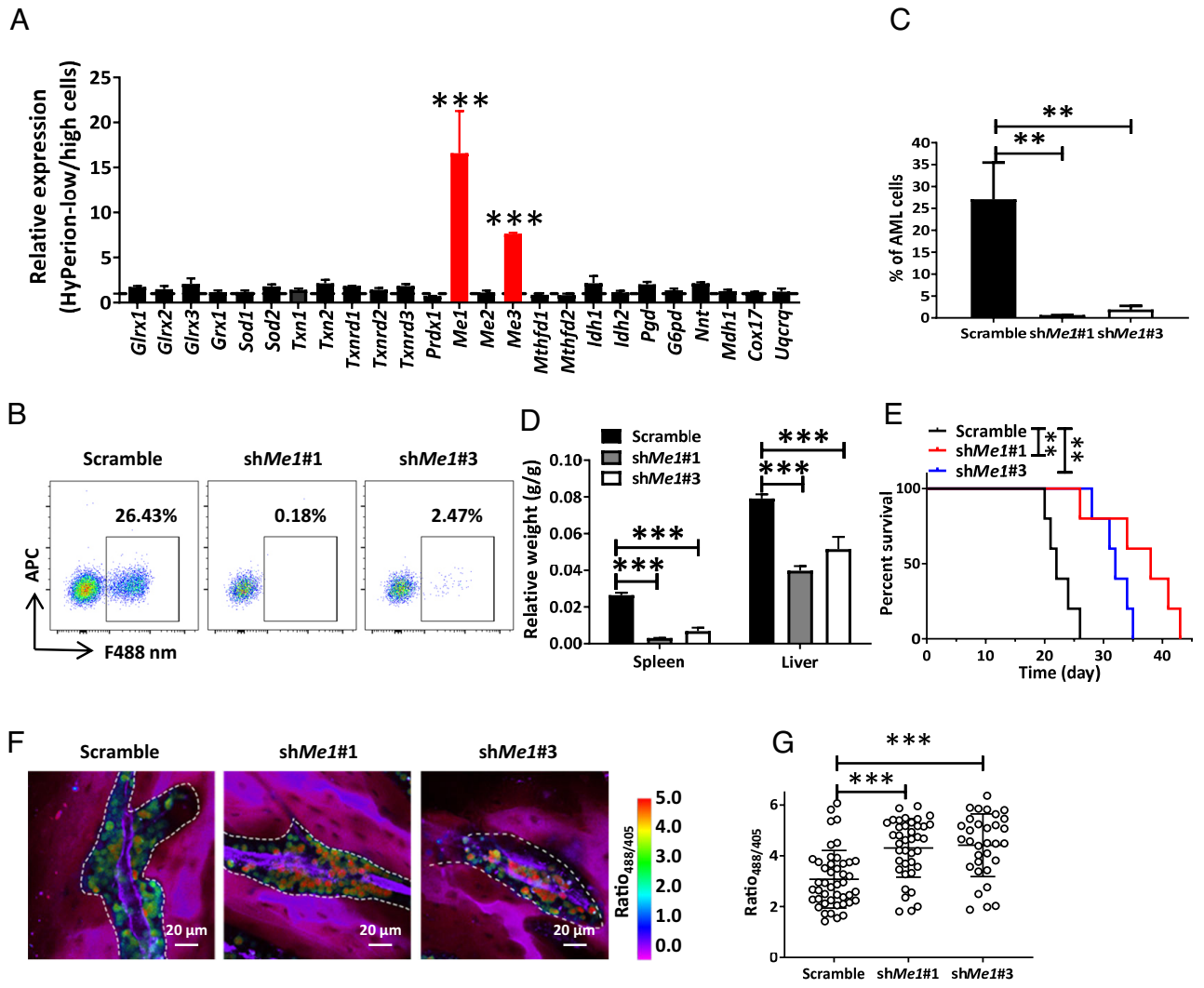

Fig. 5. ME1/3 fine-tunes H_2O_2 levels to maintain the leukemogenic capacities of HyPerion-low AML cells. (*A*) Relative mRNA expression levels of candidate changes as determined by quantitative RT–PCR in HyPerion-low and HyPerion-high AML cells. Potential downstream targets are highlighted in red (n = 3). (*B*) Representative flow cytometric analysis of the leukemia cell frequencies in the peripheral blood of recipients receiving scrambled and *Me1*-knockdown AML cells (sh*Me1*#1 and sh*Me1*#3). (*C*) Quantification of the data in Panel *B* (n = 5). (*D*) Relative weights of spleens and livers of recipients receiving *Me1*-knockdown (sh*Me1*#1 and sh*Me1*#3) or scrambled AML cells 3 wk posttransplant (n = 3). (*E*) Overall survival was determined in recipients receiving scrambled and Me1-knockdown AML cells (sh*Me1*#1 and sh*Me1*#3; n = 5). (*F*) Representative images of localizations of AML cells in the endosteal (dashed lines) and vascular niche (VE-Cad, purple) of recipients receiving *Me1*-knockdown or scrambled AML cells (sh*Me1*#1 and sh*Me1*#3). (*G*) Quantification of the data in Panel *F* (n = 5). Data are represented as means ± SD. $^{**}P < 0.01$, $^{***}P < 0.001$.

the control group (*SI Appendix*, Fig. S6 *G–I*). These findings support our notion that Ara-C-induced drug resistance is mediated by ME1/3 in MLL-AF9 AML.

Human Primary HyPerion-low AML Cells Have Enhanced Leukemogenic Capacities. We eventually sought to evaluate whether ROS levels are important for the maintenance of the leukemogenic abilities of human primary AML cells. We then overexpressed the HyPerion sensor in several human AML samples and transplanted them into nonobese diabetic/severe combined immunodeficient (NOD-SCID) mice to establish a xenograft AML model. In general, the frequencies of $CD34^+$ AML cells in these samples were also evaluated (*SI Appendix*, Fig. S7*A*). The transduced efficiencies of AML cells ranged from 25.01 to 89.53% (*SI Appendix*, Fig. S7*B*) and the engraftment levels of the NOD-SCID mice transplanted with three patient samples were 44.72%, 22.28%, and 69.41% before killed, respectively (*SI Appendix*, Fig. S7*C*). No $CD3^+$ T cells were detected in transduced $HyPerion^+$ AML cells as determined by flow cytometry (*SI Appendix*, Fig. S7*D*). We observed that three AML cell populations with low-high HyPerion ratios indeed existed in these AML cells (*SI Appendix*, Fig. S7 *E* and *F*). These AML cells also sensitively responded to the stimulation of H_2O_2, DTT, and NAC as determined by confocal microscopy (Fig. 7 *A* and *B* and *SI Appendix*, Fig. S7*G*) and flow cytometric analysis (*SI Appendix*, Fig. S7 *H* and *I*). The closer to the endosteal niche AML cells localized, the lower the HyPerion ratios the cells had. In contrast, the farther away from the vascular niche AML cells localized, the lower the HyPerion ratios the cells had (Fig. 7 *C–E* and *SI Appendix*, Fig. S7 *J–M*).

To assess whether human LICs have similar metabolic status, we analyzed patient samples with the correlation of the sensor with CD34 and CD38 immunophenotype and found much higher percentages of $CD34^+CD38^-$ cells in the HyPerion-low subset compared to those in the HyPerion-high (*SI Appendix*,

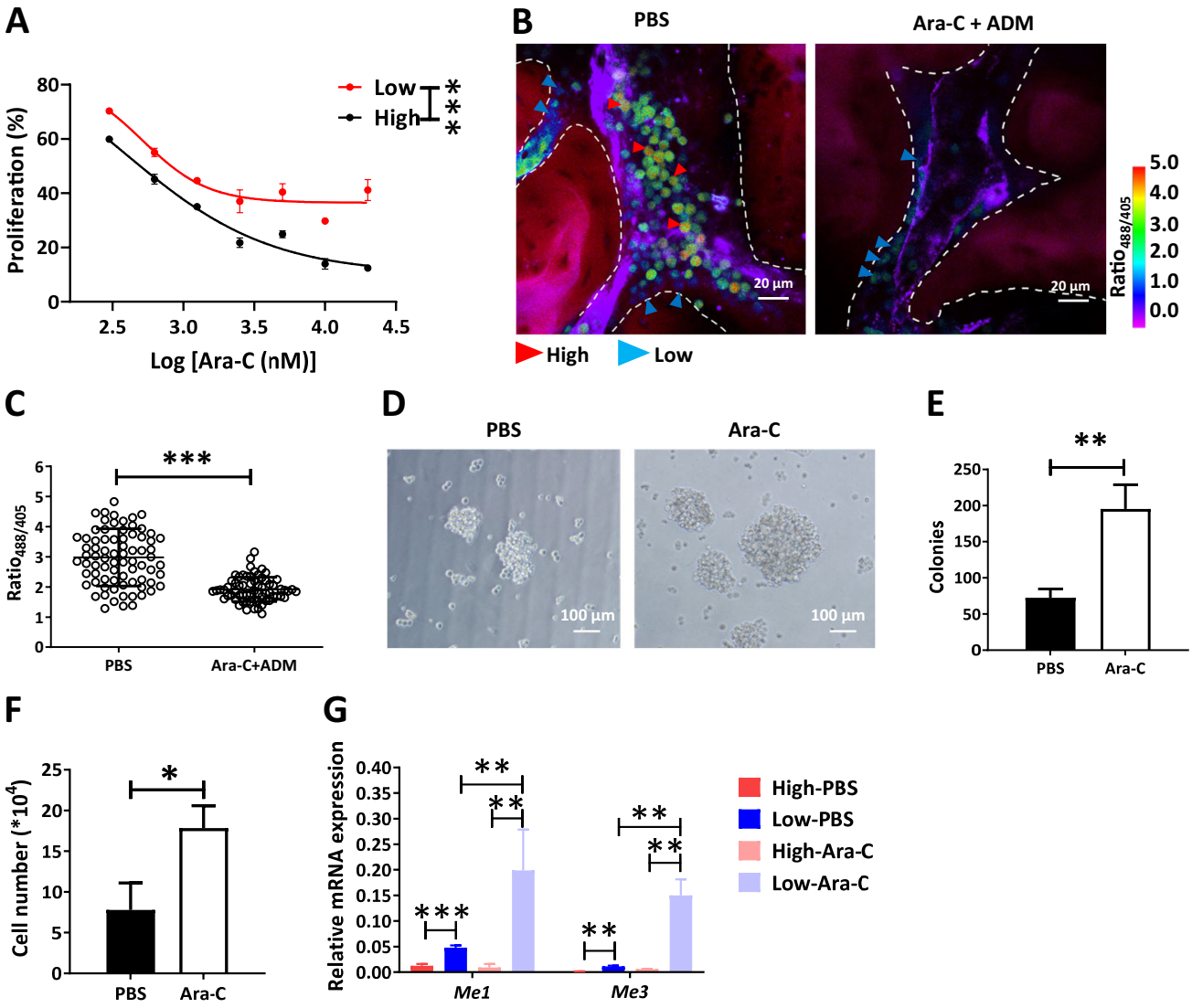

Fig. 6. HyPerion-low AML cells are more resistant to chemotherapy. (*A*) The IC50 value was determined in HyPerion-low and HyPerion-high AML cells treated with Ara-C for 72 h (n = 3). (*B*) Representative images of localizations of HyPerion^{+} AML cells in the endosteal (dashed lines) and vascular niches (VE-Cad, purple) of recipient mice. (*C*) Quantification of data for the HyPerion ratios of AML cells in Panel *B* (n = 5). (*D*) Representative images of colonies in methylcellulose medium upon PBS or Ara-C treatment. (Scale bar, 100 μm.) (*E* and *F*) Quantification of colony numbers and total cell numbers derived from HyPerion-low and HyPerion-high AML cells in Panel *D* (n = 3). (*G*) Relative mRNA levels of *Me1* and *Me3* were analyzed in HyPerion-low and HyPerion-high AML cells upon PBS or Ara-C treatment by quantitative RT-PCR analysis (n = 3). Data are represented as means ± SD. **P* < 0.05, ***P* < 0.01, ****P* < 0.001.

Fig. S7*N*), indicating that LICs were enriched in Hyperion-low subpopulation. In addition, Hyperion-low AML cells had much lower ROS levels as indicted by CellROX than that of Hyperion-high counterparts in human AML primary cells (*SI Appendix*, Fig. S7 *O* and *P*), which implied that HyPerion-low AML cells shared certain similar redox metabolic features as those CellROX-low cells.

Human HyPerion-low and HyPerion-high cells were then isolated (Fig. 7*F* and *SI Appendix*, Fig. S7 *Q–S*) and subjected to the in vitro colony assay, which showed that HyPerion-low cells generated more colonies and total derived cell amounts than HyPerion-high cells (Fig. 7 *G–I*). Moreover, in vivo transplantation experiments further revealed that the recipient mice receiving HyPerion-low cells had much higher cell frequencies in peripheral blood and reduced overall survival compared to those transplanted with HyPerion-high cells (Fig. 7 *J* and *K* and *SI Appendix*, Fig. S7 *T* and *W*). We further performed serial transplantation with patient AML samples and found that the recipient mice receiving HyPerion-low cells had a more severe leukemia burden than HyPerion-high control mice, as displayed by higher leukemia cell frequencies in peripheral blood (*SI Appendix*, Fig. S7*X*) and reduced overall survival (*SI Appendix*, Fig. S7*Y*), indicating that HyPerion-low cells were enriched for more functional LICs. In addition, we examined the expression levels of *ME1* and *ME3* in human primary HyPerion-low and HyPerion-high AML cells (AML#1-#3) by quantitative RT-PCR. HyPerion-low AML cells exhibited much higher level of *ME1* and *ME3* as compared to HyPerion-high cells (*SI Appendix*, Fig. S7*Z*), which were consistent with the findings in murine AML cells. Taken together, we demonstrated that HyPerion may act as a sensitive and specific indicator for the redox status and cell-fate determinations of LICs, which is fine-tuned by ME1/3 levels.

In summary, we established a bright genetically encoded biosensor for H_2O_2 (HyPerion) and its transgenic mouse line, which was able to precisely monitor the dynamic changes of redox metabolism in hematopoietic cells and AML cells. AML cells were very

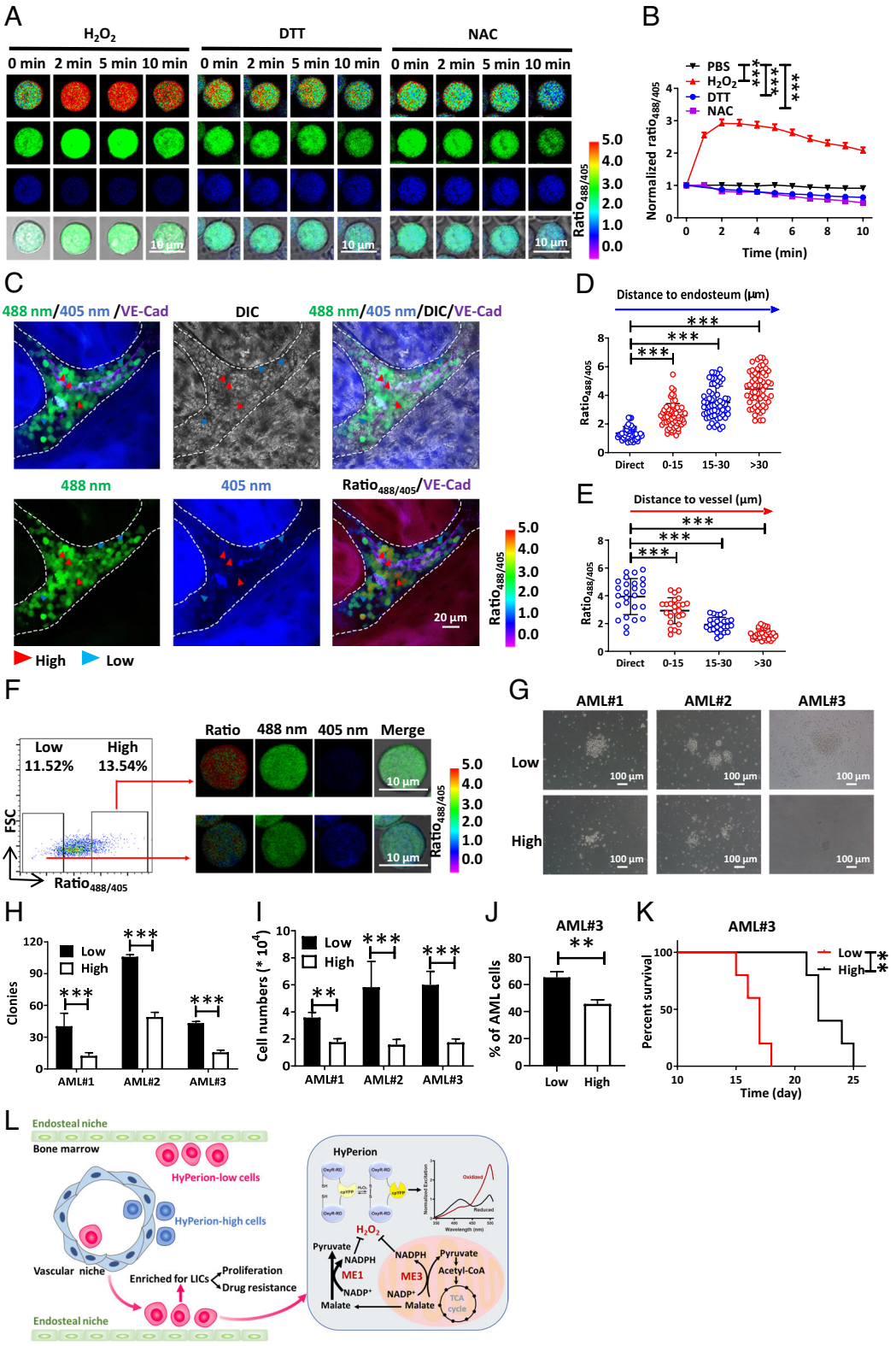

Fig. 7. Human primary HyPerion-low AML cells have enhanced leukemogenic capacities. (*A*) Representative images of the ratios of HyPerion fluorescence with excitation at 405 nm and 488 nm ($F_{488/405}$) in human primary AML cells at the indicated time points upon H_2O_2, DTT, or NAC stimulation. (*B*) Quantification of the ratios of HyPerion fluorescence in Panel *A*. A total of 35 to 50 human primary AML cells were analyzed (AML #3, n = 3). (*C–E*) Representative images of the localizations of HyPerion$^+$ human primary AML cells in the vascular niche labeled by anti-VE-cadherin antibodies (VE-Cad, purple) or in the endosteal niche (dashed lines) and their ratios of HyPerion fluorescence ($F_{488/405}$) are shown (AML #3, n = 5). (*F*) FACS-purified HyPerion-low and HyPerion-high human primary AML cells were evaluated with respect to the ratios of HyPerion fluorescence with excitation at 405 nm and 488 nm by confocal microscopy, and representative images are shown. (*G*) Representative images of colonies derived from HyPerion-low and HyPerion-high human primary AML cells cultured in methylcellulose medium. (Scale bar, 100 μm.) (*H* and *I*) Quantification of colony numbers and total cell numbers derived from HyPerion-low and HyPerion-high human primary AML cells in Panel *G* (n = 3). (*J*) The leukemia cell frequencies in peripheral blood of recipients receiving HyPerion-low and HyPerion-high human primary AML cells (AML #3, n = 5). (*K*) Overall survival was determined in recipients receiving HyPerion-low and HyPerion-high human primary AML cells in one representative experiment (AML #3, n = 5). (*L*) The working model related to the potential connections between H_2O_2 levels (ROS levels) as determined by a HyPerion sensor and cell fates of AML cells. Data are represented as means ± SD. $^{**}P < 0.01$, $^{***}P < 0.001$.

heterogeneous in H_2O_2 levels as indicated by HyPerion ratios, and HyPerion-low were more enriched for functional LICs. H_2O_2 levels were tightly connected with cell fates of AML cells including proliferation, niche localization, and drug resistance, which are fine-tuned by ME1/3-mediated NADPH generation (Fig. 7*L*). This work provides a powerful tool for in vivo monitoring ROS levels at single-cell resolution, especially for stem cells with rare frequencies, and reveals a pivotal role of redox metabolism in leukemogenesis and a potential therapeutic target.

Discussion

In the current study, we showed the redox heterogeneity of AML cells and the pathological consequences. To do this, we developed HyPerion, a bright genetically encoded H_2O_2 sensor, and engineered a transgenic mouse. These powerful tools allowed us to monitor the H_2O_2 level at single-cell resolution in vivo. The redox states of cells are dynamically changed according to the intracellular metabolism and extracellular microenvironment, which are involved in diverse physiological activities, such as survival, apoptosis, and proliferation. Therefore, it is likely that these in situ monitoring tools at spatiotemporal resolution may facilitate the mechanistic dissection of redox biology and should be particularly useful to study rare cell types, such as stem cells, which are difficult to sufficiently enrich for traditional biochemical analysis.

According to the HyPerion reporter, AML cells had heterogeneous subpopulations and displayed distinct biological behaviors. HyPerion-low cells had much higher leukemogenic capacities and were enriched for more functional LICs and resistance to chemotherapy. These observations also held true for the clinical samples derived from AML patients. Cancer cells often have a higher ROS level than normal cells. Chemotherapy or metastasis may further induce lethal oxidative stress, and low H_2O_2 levels may confer some survival advantages to cells. The identification of potential targets of redox metabolism may be useful for enrichment of functional LICs or leukemia treatment.

It has been reported that AML cells, especially LICs, have a unique preference for localization in the BM niche, which may be tightly connected with their proliferation or self-renewal capacities (11, 29–30). We and other groups have reported that LICs tend to reside in the endosteal niche rather than the vascular niche, which may be determined by their intrinsic metabolic properties, such as high levels of glycolysis (31), or extrinsic cytokines or growth factors (32, 33). Herein, we further showed a markedly distinct niche distribution of HyPerion-low and HyPerion-high cells by using an innovative H_2O_2 sensor. HyPerion-low cells have higher proliferation ability, lower oxidative phosphorylation levels, higher preference of locations in endosteal niche, and more drug resistance than HyPerion-high cells. These data also suggest that this HyPerion sensor may serve as a powerful tool for monitoring the dynamic changes in ROS levels at the single-cell level both in vitro and in vivo. This sensor may be applied to the study of other types of cells, especially stem cells with rare frequencies, with respect to both physiological and pathological status. We also showed that transgenic mice may confer great advantages for the study of redox metabolism for different systems, including hematopoietic cells, immune cells, and liver or muscle cells.

Although our data seemed to be contradicted to previous studies showing that the ROS-low phenotype in AML cells with low levels of glycolysis and OCR but relatively high OXPHOS levels as indicated by the minor increase in ECAR levels after treatment with mitochondrial inhibitors (10) and chemoresistant AML cells has a metabolic phenotype characterized by high OXPHOS activity (30, 34), we have to admit that ROS contains many different types of highly reactive substances, including peroxides, superoxide, alpha-oxygen, singlet oxygen and hydroxyl radicals, and CellROX, and DCF derivatives are mainly used for the detection of total ROS and reactive nitrogen species levels (18, 35), but not individual ROS component. In contrast, HyPerion only specifically indicates hydrogen peroxide level. In addition, for both CellROX and DCF derivative-based ROS detection, unbound extraneous dyes may render the analysis susceptible to artifacts. In contrast, HyPerion sensor allows real-time and reversible monitoring of H_2O_2 level, with a response time of seconds or less. Therefore, the metabolic properties of HyPerion-low AML cells may be not exactly the same as the ROS-low cells as indicated by CellROX. It also suggests that different subtypes of ROS components may play differential effect in the individual stage during leukemogenesis. More efforts are required to delineate the potential roles of each ROS component in leukemia development.

Numerous pathways related to ROS generation and scavenging have been reported to be important in redox balance, such as P53, Nrf2, PI3K-ATK, NF-Kb, Hif1a, Myc, and mTOR (15, 36). NADPH generated by both cytosolic ME1 and mitochondrial ME3 is one of the fundamental reducing powers for detoxification of free radicals (37). In this study, we showed that AML cells rely heavily on both ME1- and ME3-mediated NADPH generation pathways to maintain ROS levels and drive leukemogenesis. However, how ME1 and ME3 are up-regulated in HyPerion-low cells to enhance leukemogenesis is not fully addressed in the current study, and we are currently working on this topic. In addition, it has been reported that ME2 plays a vital role in AML development by Scadden's group (38). However, ME2 is a mitochondrial enzyme that mainly catalyzes the conversion of malate to pyruvate using NAD^+ as a cofactor rather than $NADP^+$ to generate NADH, which has no effect on the clearance of ROS. ME1 and ME3 use $NADP^+$ as a cofactor to generate NADPH, which serves as the major antioxidant source to decrease the ROS level. Therefore, it seemed to be reasonable that we observed that ME1 and ME3, but not ME2, were highly up-regulated in the HyPerion-low cells. These data also indicate that ME members may promote leukemogenesis through different signaling pathways and simultaneously targeting ME members may be more efficient to eradicate the leukemia cells. Moreover, the identification of potential targets related to redox metabolism may be another unique angle for the development of unique strategies for leukemia treatment, especially for overcoming chemotherapy resistance. It is also conceivable that targeting redox metabolism may be an efficient way to treat a variety of hematopoietic or solid cancers.

Methods and Materials

Mice. HyPerion construct contains the regulatory domain of the H_2O_2 sensing protein OxyR of *E. coli* and circularly permuted yellow fluorescent protein (cpYFP), and the OxyR protein acts as the element for sensing H_2O_2. To generate HyPerion transgenic mice, HyPerion was inserted into the Gt (reverse orientation splice acceptor (ROSA)) 26S or locus by the CRISPR/Cas9 technique. The preliminary preparation of the experiment was to design the guide-RNA target sequence for the genome of the target site and construct the donor DNA recombinant plasmid for the recombination of the target fragment. Guide-RNA was designed for the first intron of Rosa26 (gRNA sequence: GGCAGGCUUAAAGGCUAACCUGG). Donor DNA plasmid vector contains 3.3 kb 5′ homologous arm, CAG promoter, HyPerion-polyA, and 3.3 kb 3′ homologous arm. Cas9 mRNA, gRNA, and donor DNA were linearized, purified, and microinjected into the zygotes of C57BL/6J mice. F0 generation of Hyperion mice was further verified at the DNA and mRNA levels by PCR and quantitative RT-PCR and crossed with C57BL/6J to obtain F1 generation. In the current study, homozygote transgenic HyPerion mice were used for all the experiments. Mice were crossed and genotyped by PCR assay (primers are listed in *SI Appendix*, Table S1). Homozygous transgenic HyPerion mice were used for most of the experiments in the current study. C57BL/6 CD45.2 mice and

NOD-SCID mice were purchased from Shanghai SLAC Laboratory Animal Co. Ltd. Animal experiments were performed in accordance with the Institutional Animal Care and Use Committee of Shanghai Jiao Tong University School of Medicine.

Study Approval. Human samples were provided by the Department of Hematology of First People's Hospital or Xinhua Hospital at Shanghai Jiaotong University. This study was approved by the medical research ethics committee (Institutional Review Board (IRB)) at Shanghai Jiaotong University School of Medicine. Written informed consent was obtained from every participant. All the other experimental details can be found in *SI Appendix*.

Data, Materials, and Software Availability. All study data are included in the article and/or *SI Appendix*.

ACKNOWLEDGMENTS. This work was supported by grants from National Basic Research Program of China (2019YFA0801800, 2019YFA0904800, and 2018YFA0107000), National Natural Science Foundation of China (NSFC) (81825001, 32150030, 32030030, 32030065, 31971052, 81900147, 32121005, 92049304, 82000147, 32100906, 82170175, 82200172, and 31900833), the innovative group of NSFC (81721004), Shanghai Science and Technology Commission (19XD1422100, 20ZR1430900, 20JC1410100, 20JC1412000, 20204Y0008, and 17ZR1415500), Shanghai Frontiers Science Center of Optogenetic Techniques for Cell Metabolism, Research Unit of New Techniques for Live-cell Metabolic Imaging (Chinese Academy of Medical Sciences, 2019RU01, 2019-I2M-5-013), Major Program of Development Fund for Shanghai Zhangjiang National Innovation Demonstration Zone (Stem Cell Strategic Biobank and Stem Cell Clinical Technology Transformation Platform, ZJ2018-ZD-004), National Postdoctoral Science Foundation of China (2021T140454), Innovative research team of high-level local universities in Shanghai, the Fundamental Research Funds for the Central Universities, Chinese Academy of Medical Sciences (CAMS) Innovation Fund for Medical Sciences (2019-I2M-5-051), and Shanghai Frontiers Science Center of Cellular Homeostasis and Human Diseases.

Author affiliations: [a]Hongqiao International Institute of Medicine, Shanghai Tongren Hospital, Key Laboratory of Cell Differentiation and Apoptosis of Chinese Ministry of Education, Shanghai Jiao Tong University School of Medicine, Shanghai 200025, China; [b]Optogenetics & Synthetic Biology Interdisciplinary Research Center, Shanghai Frontiers Science Center of Optogenetic Techniques for Cell Metabolism, State Key Laboratory of Bioreactor Engineering, School of Pharmacy, East China University of Science and Technology, Shanghai 200237, China; [c]Department of Biochemistry and Molecular Cell Biology, Shanghai Key Laboratory for Tumor Microenvironment and Inflammation, Shanghai Jiao Tong University School of Medicine, Shanghai 200025, China; [d]Department of Immunology and Microbiology, Shanghai Jiao Tong University School of Medicine, Shanghai 200025, China; [e]Research Unit of New Techniques for Live-Cell Metabolic Imaging, Chinese Academy of Medical Sciences, Beijing 100730, China; [f]Shanghai Key Laboratory of Reproductive Medicine, Shanghai Jiao Tong University School of Medicine, Shanghai 200025, China; and [g]Department of Pathophysiology, Research Unit of Stress and Cancer Chinese Academy of Medical Sciences, Shanghai Cancer Institute, Renji hospital, Shanghai Jiao Tong University School of Medicine, Shanghai 200127, China

1. H. Döhner *et al.*, Diagnosis and management of acute myeloid leukemia in adults: Recommendations from an international expert panel, on behalf of the European leukemianet. *Blood* **115**, 453–474 (2010).
2. H. Döhner, D. J. Weisdorf, C. D. Bloomfield, Acute myeloid leukemia. *N Engl. J. Med.* **373**, 1136–1152 (2015).
3. P. Bose, P. Vachhani, J. E. Cortes, Treatment of relapsed/refractory acute myeloid leukemia. *Curr. Treat. Options Oncol.* **18**, 17 (2017).
4. D. Bonnet, J. E. Dick, Human acute myeloid leukemia is organized as a hierarchy that originates from a primitive hematopoietic cell. *Nat. Med.* **3**, 730–737 (1997).
5. T. Lapidot *et al.*, A cell initiating human acute myeloid leukaemia after transplantation into SCID mice. *Nature* **367**, 645–648 (1994).
6. C. L. Jones *et al.*, Inhibition of amino acid metabolism selectively targets human leukemia stem cells. *Cancer Cell* **34**, 724–740.e724 (2018).
7. Y. Tabe, M. Konopleva, M. Andreeff, Fatty acid metabolism, bone marrow adipocytes, and AML. *Front. Oncol.* **10**, 155 (2020).
8. D. Hanahan, R. A. Weinberg, Hallmarks of cancer: The next generation. *Cell* **144**, 646–674 (2011).
9. D. C. Wallace, Mitochondria and cancer. *Nat. Rev. Cancer* **12**, 685–698 (2012).
10. E. D. Lagadinou *et al.*, BCL-2 inhibition targets oxidative phosphorylation and selectively eradicates quiescent human leukemia stem cells. *Cell Stem Cell* **12**, 329–341 (2013).
11. F. Ishikawa *et al.*, Chemotherapy-resistant human AML stem cells home to and engraft within the bone-marrow endosteal region. *Nat. Biotechnol.* **25**, 1315–1321 (2007).
12. P. S. Ward *et al.*, The common feature of leukemia-associated IDH1 and IDH2 mutations is a neomorphic enzyme activity converting alpha-ketoglutarate to 2-hydroxyglutarate. *Cancer Cell* **17**, 225–234 (2010).
13. A. Sallmyr *et al.*, Internal tandem duplication of FLT3 (FLT3/ITD) induces increased ROS production, DNA damage, and misrepair: Implications for poor prognosis in AML. *Blood* **111**, 3173–3182 (2008).
14. C. Lennicke, H. M. Cochemé, Redox metabolism: ROS as specific molecular regulators of cell signaling and function. *Mol. Cell* **81**, 3691–3707 (2021).
15. H. Sies, D. P. Jones, Reactive oxygen species (ROS) as pleiotropic physiological signalling agents. *Nat. Rev. Mol. Cell Biol.* **21**, 363–383 (2020).
16. V. V. Pak *et al.*, Ultrasensitive genetically encoded indicator for hydrogen peroxide identifies roles for the oxidant in cell migration and mitochondrial function. *Cell Metab.* **31**, 642–653. e646 (2020).
17. L. A. Sena, N. S. Chandel, Physiological roles of mitochondrial reactive oxygen species. *Mol. Cell* **48**, 158–167 (2012).
18. V. V. Belousov *et al.*, Genetically encoded fluorescent indicator for intracellular hydrogen peroxide. *Nat. Methods* **3**, 281–286 (2006).
19. Z. Zhang, X. Cheng, Y. Zhao, Y. Yang, Lighting up live-cell and in vivo central carbon metabolism with genetically encoded fluorescent sensors. *Annu. Rev. Anal. Chem.* **13**, 293–314 (2020).
20. Y. Zou *et al.*, Illuminating NAD(+) metabolism in live cells and in vivo using a genetically encoded fluorescent sensor. *Dev. Cell* **53**, 240–252 (2020).
21. Y. Zhao *et al.*, SoNar, a highly responsive NAD+/NADH sensor, allows high-throughput metabolic screening of anti-tumor agents. *Cell Metab.* **21**, 777–789 (2015).
22. Y. Zhao *et al.*, In vivo monitoring of cellular energy metabolism using SoNar, a highly responsive sensor for NAD(+)/NADH redox state. *Nat. Protocol.* **11**, 1345–1359 (2016).
23. R. Tao *et al.*, Genetically encoded fluorescent sensors reveal dynamic regulation of NADPH metabolism. *Nat. Methods* **14**, 720–728 (2017).
24. Y. Zou *et al.*, Analysis of redox landscapes and dynamics in living cells and in vivo using genetically encoded fluorescent sensors. *Nat. Protocol.* **13**, 2362–2386 (2018).
25. S. Trakhanov *et al.*, Ligand-free and -bound structures of the binding protein (LivJ) of the Escherichia coli ABC leucine/isoleucine/valine transport system: Trajectory and dynamics of the interdomain rotation and ligand specificity. *Biochemistry* **44**, 6597–6608 (2005).
26. D. S. Bilan *et al.*, HyPer-3: A genetically encoded H2O2 probe with improved performance for ratiometric and fluorescence lifetime imaging. *ACS Chem. Biol.* **8**, 535–542 (2013).
27. K. Setsukinai, Y. Urano, K. Kakinuma, H. J. Majima, T. Nagano, Development of novel fluorescence probes that can reliably detect reactive oxygen species and distinguish specific species. *J. Biol. Chem.* **278**, 3170–3175 (2003).
28. R. Y. Tsien, The green fluorescent protein. *Annu. Rev. Biochem.* **67**, 509–544 (1998).
29. C. R. Cogle *et al.*, Functional integration of acute myeloid leukemia into the vascular niche. *Leukemia* **28**, 1978–1987 (2014).
30. M. Ninomiya *et al.*, Homing, proliferation and survival sites of human leukemia cells in vivo in immunodeficient mice. *Leukemia* **21**, 136–142 (2007).
31. X. Hao *et al.*, Metabolic imaging reveals a unique preference of symmetric cell division and homing of leukemia-initiating cells in an endosteal niche. *Cell Metab.* **29**, 950–965 (2019).
32. D. S. Krause *et al.*, Differential regulation of myeloid leukemias by the bone marrow microenvironment. *Nat. Med.* **19**, 1513–1517 (2013).
33. S. Tavor *et al.*, CXCR4 regulates migration and development of human acute myelogenous leukemia stem cells in transplanted NOD/SCID mice. *Cancer Res.* **64**, 2817–2824 (2004).
34. N. van Gastel *et al.*, Induction of a timed metabolic collapse to overcome cancer chemoresistance. *Cell Metabol.* **32**, 391–403.e396 (2020).
35. J. P. Crow, Dichlorodihydrofluorescein and dihydrorhodamine 123 are sensitive indicators of peroxynitrite in vitro: Implications for intracellular measurement of reactive nitrogen and oxygen species. *Nitric Oxide* **1**, 145–157 (1997).
36. I. S. Harris, G. M. DeNicola, The complex interplay between antioxidants and ROS in cancer. *Trends Cell Biol.* **30**, 440–451 (2020).
37. P. Jiang, W. Du, A. Mancuso, K. E. Wellen, X. Yang, Reciprocal regulation of p53 and malic enzymes modulates metabolism and senescence. *Nature* **493**, 689–693 (2013).
38. Y. P. Wang *et al.*, Malic enzyme 2 connects the Krebs cycle intermediate fumarate to mitochondrial biogenesis. *Cell Metabol.* **33**, 1027–1041.e1028 (2021).
39. L. Poulain *et al.*, High mTORC1 activity drives glycolysis addiction and sensitivity to G6PD inhibition in acute myeloid leukemia cells. *Leukemia* **31**, 2326–2335 (2017).
40. H. Medyouf, The microenvironment in human myeloid malignancies: Emerging concepts and therapeutic implications. *Blood* **129**, 1617–1626 (2017).